16th World Congress of the International Fuzzy Systems Association (IFSA)
9th Conference of the European Society for Fuzzy Logic and Technology (EUSFLAT)

LULC database updating from VHR images and LIDAR data using evidence theory

B. Rodríguez-Cuenca[1], M.C. Alonso[1] and A. Tamés-Noriega[1]

[1]Department of Physics and Mathematics, University of Alcalá, Madrid, Spain

Abstract

Urban growth and the development of urban plans make cities grow and substantially alter, in relatively short time periods, their land covers and land uses (LULC). To take control of this urban growth, it is important to create and update the LULC database. In this work, a method to automatically extract land covers from satellite VHR imagery and LIDAR data is presented. This method is based on the Dempster-Shafer evidence theory. The efficiency of this method is tested in three test sites in the Spanish city of Gijón. The provided results are compared with the SIOSE database in order to determine changes in the LULC.

Keywords: Evidence theory, VHR imagery, LIDAR, pattern recognition, segmentation

1. INTRODUCTION

The automatic detection of land use and land cover (LULC) from remote sensing data has been established as an indispensable tool for providing adequate and accurate information for natural resource management, sustainable development for decision makers and the evaluation of urban expansion and land use change [1]. LULC changes are one of the main factors influencing the evolution of landscapes; it is important to detect these changes as automatically as possible. The first works toward the LULC extraction were made by photointerpretation. These works were very expensive because they were time-consuming and their accuracy depended on the experience of the operator. The technological advances of the last two decades have provided very high resolution (VHR) sensors, both spatial and spectral, and the incorporation of laser technology to remote sensing issues through the LIDAR data. As long as remote sensing data increases its quality and quantity, several methods can be used to automatically detect the change in the LULC of different landscapes. In [2], a method to classify land covers from airborne LIDAR data is presented, while a classification of urban land covers from high spatial resolution imagery is carried out in [3]. However, it is hard to find an appropriate method to detect LULC in every region, especially in urban areas where different types of confluence uses take place (residential, commercial, industrial and leisure). The main goal of LULC detection works is to automate the detection process as much as possible, minimizing the mediation of human operators. Several works based on thresholding or classification algorithms have tried to automate the LULC detection from remote sensing data. The thresholding method consists of using the spectral behavior of every LULC object in order to detect it from aerial or satellite images. Thresholding establishes a decision rule in every considered decision index that allows for determining the location of every LULC object considered. The most common way to apply the decision rules is by using a decision tree [4]. Otherwise, image classification consists of dividing an image into different classes using some a priori information about the spectral behavior of every considered land cover. While several algorithms can be used to perform a classification, the most widely used classification algorithms include Support Vector Machine (SVM) and neural network algorithms. Examples of some of the studies that have used classification algorithms to detect LULC are: [5], which compares the performance of SVM, maximum likelihood and artificial neural networks to classify both multispectral and hyperspectral imagery, or [6], which fuses hyperspectral images and LIDAR data for classify complex forest areas using SVM.

The work presented in this paper is focuses on the extraction of land covers from VHR satellite images and LIDAR data to create and update a LULC database. It starts with a segmentation process carried out on the satellite image followed by a rasterization of the LIDAR data. From the input information, four decision indexes are computed, and through the Dempster-Shafer evidence theory, every region of the segmented image is labelled as high vegetation, low vegetation, building, paved surface/bare soil or water surface. The paper is organized as follows: Section 2 summarizes the materials used as inputs in the presented method; in Section 3, the proposed method to extract and update LULC is detailed; and Section 4 shows the results obtained in three test sites and a comparison with SIOSE (information system on land occupation of Spain, in Spanish "Sistema de Información sobre Ocupación del Suelo en España") database. Finally, our conclusions and future works are described in Section 5.

2. MATERIAL

In this work, a very high resolution (VHR) satellite imagery and LIDAR data were used as inputs. The VHR image corresponds to a WorldView2 sensor, which provides information in eight spectral bands, six from the optical spectrum and two from the infrared wavelengths: coastal (400–450nm), blue (450–510 nm), green (510–580 nm), yellow (585–625 nm), red (630–690 nm), red edge (705–745 nm), near infrared 1 (770–895 nm) and near infrared 2 (860–1040 nm). These

types of images have a spatial resolution of 0.46 m in the panchromatic band and 1.85 m in multispectral bands. In this work, the multispectral band was resampled to 2.5 m due to the resolution of the LIDAR data. The image was taken in March 2012 in the Spanish city of Gijón. The scene used in this work has a size of 2,400 x 800 pixels and covers an area of 24 square kilometers.

LIDAR technology measures distances by illuminating a target with a laser and analyzing the reflected light. The combination of a sweeping beam laser with inertial navigation systems and a GPS guarantees a high geometric precision in the data. In this study, we used the LEICA ALS50-II (Leica Geosystems AG, Heerbrugg, Switzerland) sensor to capture the LIDAR data. LIDAR data exists on a 3D point cloud that, for each point, provides not only the height information but also, among other things, the intensity of the return laser pulse, its scan angle or the time when it was registered. Taking advantage of the Z coordinate provided by LIDAR sensors, it is possible to quickly and accurately generate a digital surface model (DSM) with precision in the order of 20cm in planimetry and 30cm in height [3]. Although a DSM could also be obtained by using classical digital photogrammetry, that method would be more expensive and slower to produce. The LIDAR data used in the present work corresponds to a flight that was conducted in the summer of 2012. The flight was taken at an altitude of approximately 1,800m and with a minimum point density of 0.5 points per square meter. The coordinate system is WGS84 with orthometric heights.

(a)

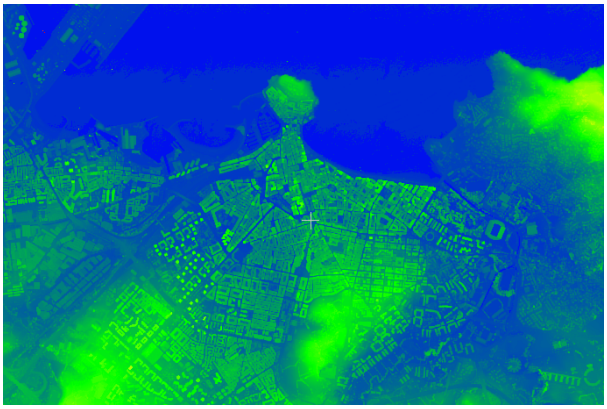

(b)

Figure 1. Aerial image of the studied area in true color RGB (a) (© European Space Imaging / DigitalGlobe) and DSM (b)

3. METHOD

In this paper, a method for the automatic updating of land use land cover (LULC) databases is presented. Five land covers have been considered in this work: paved surfaces/bare soil, water surfaces, buildings, high vegetation and low vegetation. The inputs of the procedure are VHR satellite images and LIDAR data. The identification and extraction of considered land covers began with the rasterization of the LIDAR data and the creation of a digital terrain model (DTM) and a DSM. After that, a segmentation of the satellite image was carried out in order to perform the extraction at region level rather than at pixel level. The Dempster-Shafer evidence theory was applied to determine which category corresponds to each region of the segmented image according to four decision indexes that have been considered. Fig. 2 shows a flow chart of the method proposed in this paper.

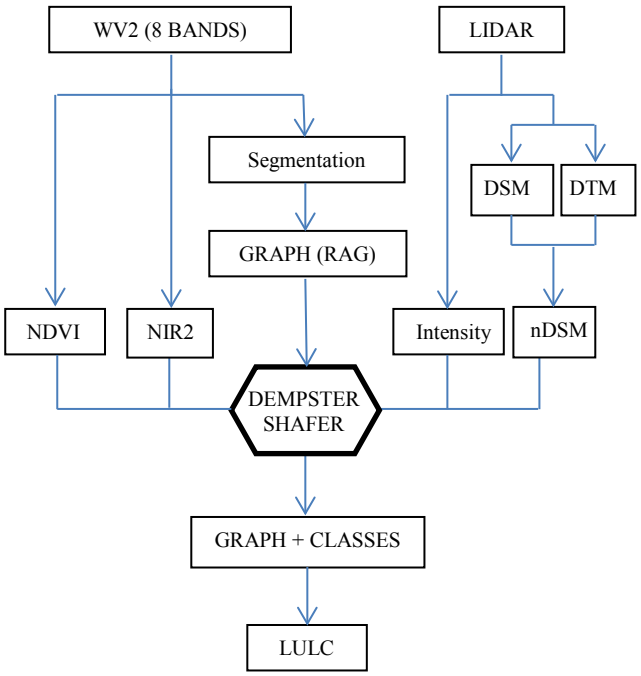

Figure 2. Flow chart of the proposed method

3.1. Image segmentation

The first step in the procedure was the reading of the different bands involved in the process. In the VHR satellite image, three optic bands—red (R), green (G) and blue (B)—and two near infrared bands—NIR1 and NIR2—were used. On these input bands, a segmentation process was applied. This consisted of group pixels that had similar properties as super-pixels or segments. Those pixels that belong to the same segment were treated as a set. The object of a segmentation process is to simplify the appearance of an image in order to make it more meaningful and easy to analyze. Several meth-

ods can be used for segmenting, such as, among others, clustering, mean-shift and thresholding. In this work, a region growing procedure was the selected method used to carry out the segmentation [7]. The region growing segmentation method was applied to a single band. However, images used in this work were multispectral imagery composed of several bands. To consider a single band, a Principal Component Analysis (PCA) was applied on the eight bands of the satellite image. The first component of the PCA, which represents the highest variability, is that on which the segmentation process is applied.

3.2. Decision indices

Four decision indexes were studied to detect the considered land cover existing in the studied area, as follows:

NDVI: the normalized difference vegetation index (NDVI) (1) is a well-known index in remote sensing. It is useful to determine the quantity, quality and vegetation growth from aerial images taken by remote sensing. In the NDVI index, vigorous vegetation has high values. The NDVI index has widespread use in different remote sensing applications [8, 9].

$$NDVI = \frac{NIR1 - RED}{NIR1+RED} \qquad (1)$$

nDSM: from the rasterization of the height information contained in the LIDAR data, two new products were generated: the DSM and the DTM. The DSM was obtained from the first echo of each pulse after filtering the noise that was generated in the process of data capture. The DSM contained information regarding construction, vegetation and uncultivated ground. The DTM was generated as a product derived from the DSM after employing a semi-automatic method developed by [10]. Finally, calculation of the difference between the DSM and the DTM generated the standard DSM (nDSM, normalized digital surface model). In the nDSM, every man-made construction in the field is represented. This model is very useful for detecting and differentiating land constructions and height elements.

LIDAR intensity: in addition to providing information related to the Z-coordinate, LIDAR data provides other information, such as the intensity of the return pulses or the scan angles. As the height information, intensity was rasterized and the final intensity of each pixel was calculated as the average of all LIDAR points contained in each cell. Intensity values are low in rough surfaces (with diffuse reflection), such as paved areas. This behavior is used to extract paved surfaces and bare soil.

NIR: WorldView2 imagery provides information in two different ranges of wavelengths of the near infrared (NIR) spectrum. Some land covers have a characteristic spectral response in these wavelengths. While vegetation areas have a high value in these bands, water surfaces present a high absorption, which is useful to extract these covers.

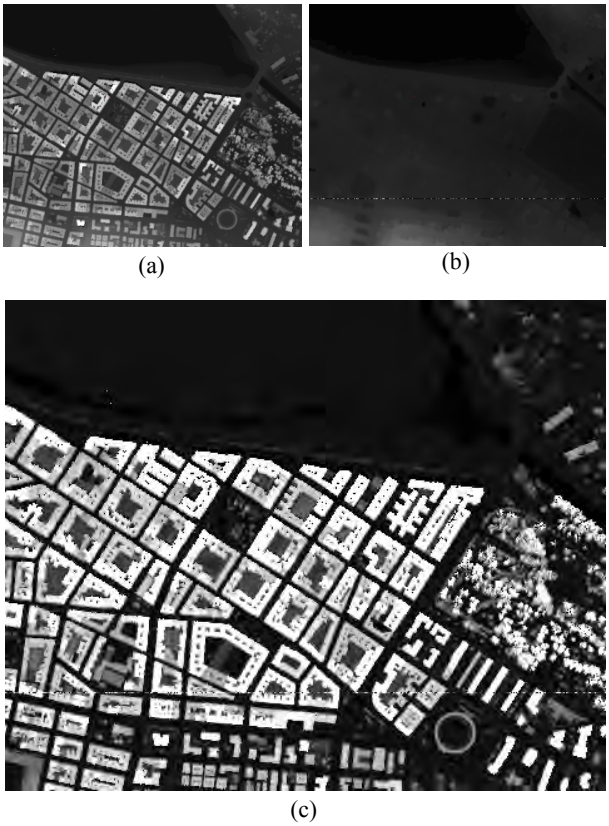

(a) (b)

(c)

Figure 3. Detail of the (a) digital surface model, (b) digital terrain model and (c) normalized digital surface model of the studied area

3.3. Evidence theory

Once the four indexes are calculated, decision thresholds are set for each index and the evidence theory is applied. The mathematical theory of evidence is a field in which data sources are treated separately, and their contributions are combined to provide a joint inference on the correct label for every pixel [11]. This theory does not require a full probability model to work against the requirements of other approaches. It tries to benefit from the utilization of sets of assumptions or hypotheses rather than to address a hypothesis or an assumption separately, as is done in other approaches.

Evidence theory is applied to each of the segmented image regions. The result of this process is, for every region, the probability of belonging to each of the five considered classes. Each region is classified in the category with the highest probability of belonging according to the Dempster-Shafer applied.

3.3.1 Dempster–Shafer Theory in Land Cover Detection

The objective of the current work is the creation of a map with the location of five considered land covers: buildings, vegetation, roads, bare soil and water surfaces. In the Dempster–Shafer evidence theory implemented in this work, the building class is noted with X and vegetation with Y; Z corresponds to roads; T is reserved for bare soil and W for water surfaces. Also considered is θ as the inherent uncertainty in the theory of evidence. The frame of discernment, Ω, is formed by X, Y, Z, T, W and θ:

$$\Omega = \{X, Y, Z, T, W, \theta\}$$

For each decision index, mass of evidence are noted by μ_i (i = 1…4, number of decision indices considered): ($\mu_i(X)$,$\mu_i(Y)$,$\mu_i(Z)$,$\mu_i(T)$,$\mu_i(W)$,$\mu_i(\theta)$ with the assumption that $\mu_i(X)+ \mu_i(Y)+ \mu_i(Z)+\mu_i(T)+ \mu_i(W)+\mu_i(\theta)=1$, $\forall i = 1\ldots 4$ [12]. The probability of belonging to each category ($\mu_i(X)$,$\mu_i(Y)$,$\mu_i(Z)$,$\mu_i(T)$,$\mu_i(W)$,$\mu_i(\theta)$) are determined from the values taken by each index on every region according to some functions developed by the authors. Thus, a high NDVI value corresponds to a high probability of belonging to vegetated land cover and a low probability of belonging to the remaining land cover.

With the values $\mu_i(X)$,$\mu_i(Y)$,$\mu_i(Z)$,$\mu_i(T)$,$\mu_i(W)$,$\mu_i(\theta)$ for the four decision indices (i = 1 …4), the evidence combination rule of Dempster-Shafer is applied for every region in the image [13]. This combination (μ_{ij}) is an iterative process in which the knowledge acquired with a certain rate (μ_i) is combined with the following index (μ_j) (2):

$$\mu_{ij} = (\mu_i \otimes \mu_j)(A) = \frac{\sum_{B \cap C = A} \mu_i(B)\, \mu_j(C)}{\sum_{B \cap C \neq \varnothing} \mu_i(B) \mu_j(C)} \qquad (2)$$

The result of this process is, for every region, the probability of belonging to each of the considered categories.

4. RESULTS

To determine the accuracy of the proposed method, it was applied to the 2012 dataset, which comprises 24 km^2 (Figure 4). The achieved results were tested in three polygons whose LULC are available in the SIOSE (information system of land occupation in Spain) database. This database was collected in 2005. In it, Spain is divided into small polygons for each of which the percentage of land cover is known by photointerpretation techniques. To evaluate the accuracy of the detected land covers in these three polygons, the achieved results were compared with the SIOSE database. Thus, we can check the efficiency of the method and verify in which polygons were there changes in the land covers in seven years (2005 to 2012).

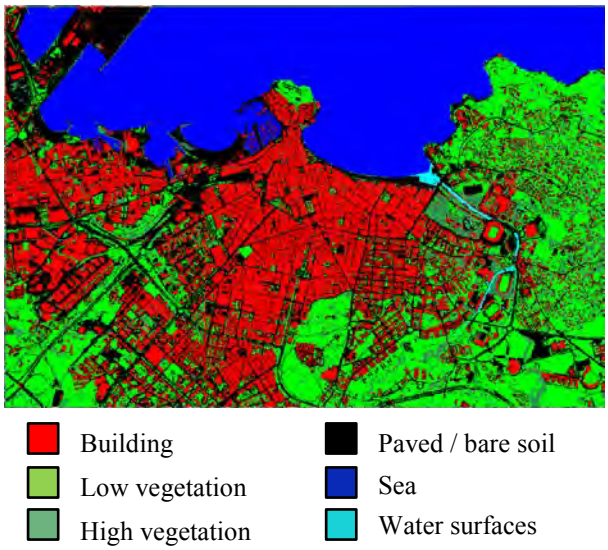

Figure 4: LULC extracted in the 24 km^2 studied dataset

(a)

(b)

Figure 5. Test site 1: (a) polygon superimposed on the RGB-mode image and (b) LULC extracted with the proposed method

Test Site 1: this test site represents more than 10 hectares of the city center where there are buildings and small parks with wooded areas organized in an orthogonal structure of roads and streets (Figure 5).

The results of the extraction in this polygon are shown in Table 1. There have been no major urban developments in this area between the studied dates. As can be seen in Table 1, according to the SIOSE database, 35% of the surface of this polygon corresponds to buildings, more than 5% to vegetation and almost 60% to paved surface and bare soil. The proposed method provides similar results, with 46% buildings, 12.5% vegetation (divided into 9% low vegetation and 3.5% wooded areas) and 41.5% paved surfaces and bare soil. Small variations have been observed in the buildings and paved/bare soil classes. These differences could be due to small changes in this neighborhood between the

Test Site 1		
	Demster-Shafer	SIOSE
Buildings	46%	35%
Low Vegetation	9%	7%
Paved/bare soil	41.5%	58%
High vegetation	3.5%	0%

Table 1: percentage of every LULC detected by the proposed method and in SIOSE database

dates of study or to errors in the creation of SIOSE database.

Test Site 2: this polygon represents an expansion of the city, an area of growth which has undergone significant urban changes. This test site has a size of 6.6 hectares and it is comprised of grassland combined with developed plots connected with a road (Figure 6). According to the SIOSE dataset, this polygon is 5% buildings, 45% paved/bare soils and 50% areas of extraction. These results are very different from those obtained by the proposed method, which stated that the polygon was 31.3% buildings, 32% vegetation and 36.7% paved/bare soil (Table 2). These differences are due to the fact that, in 2005, when SIOSE database was done, this polygon was an area where some plots were empty and others were under construction (Figure 6 (a)). In 2012, all works were completed and the area had a completely different look (Figure 6 (b)). This test site is useful to show the potential of the proposed method to detect those areas of the city where there has been urban growth.

(a)

(b)

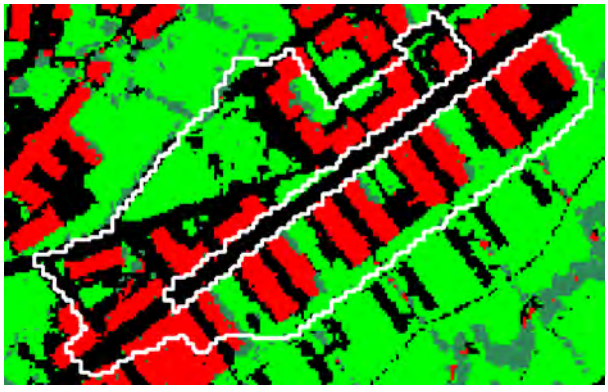

(c)

Figure 6. Test site 2: (a) polygon superimposed on the RGB-mode image in 2006 and (b) in 2013. (c) LULC extracted with the proposed method

Test Site 2		
	Demster-Shafer	SIOSE
Buildings	31.3%	5%
Low Vegetation	28.8%	0%
Paved/bare soil	36.7%	45%
High vegetation	3.2%	0%
Extraction area	0%	50%

Table 2: percentage of every LULC detected by the proposed method and in SIOSE database

Test Site 3: this polygon has a size of 4.4 hectares and is located on the outskirts of the city, away from residential areas, and it is not included in any urban growth plan. Nevertheless, in the SIOSE database, it is shown that this polygon is 15% buildings, 25% paved/bare soil and 60% extraction area (Table 3). This classification is far from the one obtained by our method, which determines that 87.5% of this polygon represents vegetation (the majority, 86.8%, is low vegetation and the 0.7% is woodlands), 12.4% corresponds to paved/bare soil and buildings only represent a 0.1% (Figure 7(a)). These differences are due to the fact that this polygon has undergone major changes between 2005 and 2012. In 2005, they were conducting a series of work for the construction of an underground train station. These works were of great wingspan and during their execution, worksites and cranes were installed, which photointerpreters classified as buildings in the SIOSE database (Figure 7(b)). In 2012, the works were completed and the polygon recovered its original appearance (Figure 7(c)).

Test Site 3		
	Demster-Shafer	SIOSE
Buildings	0.1%	15%
Low Vegetation	86.8%	0%
Paved/bare soil	12.4%	25%
High vegetation	0.7%	0%
Extraction area	0%	60%

Table 3: percentage of every LULC detected by the proposed method and in SIOSE database

5. CONCLUSIONS

In this paper, a novel method to extract and classify land covers in order to update LULC databases, applying the Dempster-Shafer evidence theory on VHR satellite images and LIDAR data, is presented. The process begins with a segmentation of the satellite image and the rasterization of the information contained in the LIDAR data. The land cover extraction is based on four

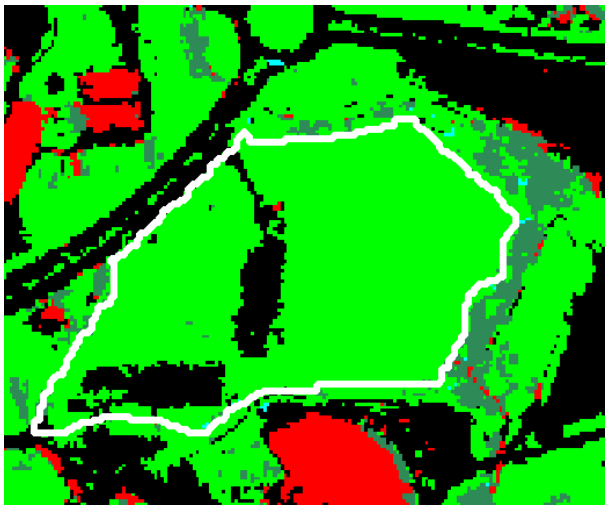

(a)

(b)

(c)

Figure 7. Test site 3: (a) LULC extracted with the proposed method, (b) polygon superimposed on an RGB-mode aerial image taken (b) in 2006 and (c) in 2013.

decision indexes, which, through the evidence theory, allow the classification of every region of the segmented image into five different classes: low vegetation, high vegetation, water surfaces, paved surfaces/bare soil and buildings. The proposed method was tested in three polygons for which land cover information is available in a database from 2005. The results obtained show the efficiency and potentiality of the proposed method to extract land covers from satellite images and LIDAR data and update LULC databases. In the future, other features and rules will be considered to add more land covers in the process of LULC extraction.

Acknowledgements

The authors would like to thank the Spanish Mapping Agency (Instituto Geográfico Nacional, IGN) for providing the LIDAR data and SIOSE database and the Spanish Ministry of Science and Innovation for financial support, Project No. CGL2010-15357/BTE

References

[1] J. Xiao, Y. Shen, J. Ge, R. Tateishi, C. Tang, Y. Liang, and Z. Huang, "Evaluating urban expansion and land use change in Shijiazhuang, China, by using GIS and remote sensing," *Landscape and urban planning,* vol. 75, pp. 69-80, 2006.

[2] A. Antonarakis, K. S. Richards, and J. Brasington, "Object-based land cover classification using airborne LiDAR," *Remote Sensing of Environment,* vol. 112, pp. 2988-2998, 2008.

[3] S. W. Myint, P. Gober, A. Brazel, S. Grossman-Clarke, and Q. Weng, "Per-pixel vs. object-based classification of urban land cover extraction using high spatial resolution imagery," *Remote Sensing of Environment,* vol. 115, pp. 1145-1161, 2011.

[4] M. A. Friedl, C. E. Brodley, and A. H. Strahler, "Maximizing land cover classification accuracies produced by decision trees at continental to global scales," *Geoscience and Remote Sensing, IEEE Transactions on,* vol. 37, pp. 969-977, 1999.

[5] M. Pal and P. Mather, "Support vector machines for classification in remote sensing," *International Journal of Remote Sensing,* vol. 26, pp. 1007-1011, 2005.

[6] M. Dalponte, L. Bruzzone, and D. Gianelle, "Fusion of hyperspectral and LIDAR remote sensing data for classification of complex forest areas," *Geoscience and Remote Sensing, IEEE Transactions on,* vol. 46, pp. 1416-1427, 2008.

[7] B. Rodriguez-Cuenca, J. A. Malpica, and M. C. Alonso, "Region-growing segmentation of multispectral high-resolution space images with open software," in *Geoscience and Remote Sensing Symposium (IGARSS), 2012 IEEE International*, 2012, pp. 4311-4314.

[8] N. Pettorelli, J. O. Vik, A. Mysterud, J.-M. Gaillard, C. J. Tucker, and N. C. Stenseth, "Using the satellite-derived NDVI to assess ecological responses to environmental change," *Trends in ecology & evolution,* vol. 20, pp. 503-510, 2005.

[9] P. S. Chavez and D. J. MacKinnon, "Automatic detection of vegetation changes in the southwestern United States using remotely sensed images," *Photogrammetric engineering and remote sensing,* vol. 60, 1994.

[10] G. T. Raber, J. R. Jensen, S. R. Schill, and K. Schuckman, "Creation of digital terrain models using an adaptive lidar vegetation point removal process,"

Photogrammetric engineering and remote sensing, vol. 68, pp. 1307-1314, 2002.
[11] B. Rodríguez-Cuenca and M. C. Alonso, "Semi-Automatic Detection of Swimming Pools from Aerial High-Resolution Images and LIDAR Data," *Remote Sensing,* vol. 6, pp. 2628-2646, 2014.
[12] J. A. Malpica, M. C. Alonso, and M. A. Sanz, "Dempster–Shafer Theory in geographic information systems: A survey," *Expert Systems with Applications,* vol. 32, pp. 47-55, 2007.
[13] A. P. Dempster, "A generalization of Bayesian inference," *Journal of the Royal Statistical Society. Series B (Methodological),* pp. 205-247, 1968.